Title
Inverse modeling of ground surface uplift and pressure with iTOUGH-PEST and TOUGH-FLAC: The case of CO2 injection at In Salah, Algeria

Authors
Rinaldi, Antonio P
Rutqvist, Jonny
Finsterle, Stefan
et al.

Publication Date
2017-11-01

DOI
10.1016/j.cageo.2016.10.009

Peer reviewed

INVERSE MODELING OF GROUND SURFACE UPLIFT AND PRESSURE WITH iTOUGH-PEST AND TOUGH-FLAC: THE CASE OF CO_2 INJECTION AT IN SALAH, ALGERIA

Antonio P. Rinaldi[(a,b)], Jonny Rutqvist[(a)], Stefan Finsterle[(a)], Hui-Hai Liu[(a,c)]

(a) Energy Geosciences Division, Lawrence Berkeley National Laboratory, Berkeley, CA, USA
e-mail: aprinaldi@lbl.gov, jrutqvist@lbl.gov, safinsterle@lbl.gov

(b) Swiss Seismological Service, Swiss Federal Institute of Technology, ETHZ, Zürich, Switzerland
e-mail: antoniopio.rinaldi@sed.ethz.ch

(c) Aramco Research Center, Houston, TX, USA
e-mail: hui-hai.liu@aramcoservices.com

(*) Corresponding author at: Swiss Seismological Service, ETHZ, Sonneggstrasse 5, Zürich, Switzerland

submitted to Comput. Geosci.

ABSTRACT

Ground deformation, commonly observed in storage projects, carries useful information about processes occurring in the injection formation. The Krechba gas field at In Salah (Algeria) is one of the best-known sites for studying ground surface deformation during geological carbon storage. At this first industrial-scale on-shore CO_2 demonstration project, satellite-based ground-deformation monitoring data of high quality are available and used to study the large-scale hydrological and geomechanical response of the system to injection. In this work, we carry out

coupled fluid flow and geomechanical simulations to understand the uplift at three different CO_2 injection wells (KB-501, KB-502, KB-503). Previous numerical studies focused on the KB-502 injection well, where a double-lobe uplift pattern has been observed in the ground-deformation data. The observed uplift patterns at KB-501 and KB-503 have single-lobe patterns, but they can also indicate a deep fracture zone mechanical response to the injection.
The current study improves the previous modeling approach by introducing an injection reservoir and a fracture zone, both responding to a Mohr-Coulomb failure criterion. In addition, we model a stress-dependent permeability and bulk modulus, according to a dual continuum model. Mechanical and hydraulic properties are determined through inverse modeling by matching the simulated spatial and temporal evolution of uplift to InSAR observations as well as by matching simulated and measured pressures. The numerical simulations are in agreement with both spatial and temporal observations. The estimated values for the parameterized mechanical and hydraulic properties are in good agreement with previous numerical results. In addition, the formal joint inversion of hydrogeological and geomechanical data provides measures of the estimation uncertainty.

Keywords: Geomechanics, CO_2 sequestration, inverse modeling, coupled modeling, TOUGH-FLAC, iTOUGH-PEST

1. INTRODUCTION

Large-scale deep underground CO_2 injection represents a viable option for reducing carbon emissions to the atmosphere (Pacala and Socolow, 2004). The feasibility of geological carbon sequestration is, however, questioned by the potential for inducing seismicity and altering the sealing capacity of a storage site (Zoback and Gorelik, 2012), despite the fact that large events in sedimentary formations are unlikely (Vilarrasa and Carrera, 2015). Notwithstanding the potential for large events, microseismic events may still occur as observed at several CO_2 projects (e.g. at

Weyburn in Canada, Decatur in USA, Lacq-Rousse in France), most of them with negative magnitude (Verdon and Stork, 2016).

The presence of microseismicity indicates that rock stress and strain vary in response to carbon dioxide injection; a coupled fluid flow and geomechanics model may provide understanding of the various processes occurring at depth (Rutqvist, 2012). Recently, several efforts aimed at developing reliable codes for the study of coupled processes occurring during deep carbon injection (e.g. Rutqvist et al., 2002; Vilarrasa et al., 2010; Rutqvist, 2011; Bissell et al., 2011; Kolditz et al., 2012; Jha and Juanes, 2014). Sufficiently accurate characterization of a carbon storage site requires the integration of a large amount of data into a predictive model. An inverse modeling approach is needed to assess the relevance of parameters for reproducing the available data, determining the error of the estimated parameters and how this uncertainty is propagated to model predictions.

In this study, we demonstrate the use of the coupled fluid flow and geomechanics inverse modeling approach by applying it to data from the In Salah CO_2 demonstration site.

The In Salah CO_2 Storage Project in Algeria was in operation between 2004 and 2011 and was the first on-shore, industrial-scale demonstration site for CO_2 sequestration. Via three injection wells (KB-501, KB-502, KB-503), about 4 million tons of carbon dioxide were injected into a 20 m thick, water-filled reservoir at a depth of about 2000 m. The three wells were drilled horizontally with a length between 1 and 1.5 km. A large caprock overburden with a thickness of about 900 m prevented the CO_2 from escaping to shallow depths (Ringrose et al., 2013).

The In Salah demonstration site is also well known for the comprehensive characterization and monitoring effort, including wellhead sampling, down-hole logging, core analysis, surface gas and groundwater aquifer monitoring, tracers, 4D seismic, and satellite InSAR data (Mathieson et al., 2011). Such InSAR data provide essential information for the development of a reliable model through the inverse analysis of coupled fluid flow and geomechanics.

In the first part of this study, we analyze the evolution of deformation and pressure at the KB-502 injection well, where a double-lobe uplift feature has been observed by analysis of satellite data. Such a feature has been explained by both semi-analytical and numerical modeling as the opening of a deep fracture (Vasco et al., 2010; Rutqvist et al., 2011; Rinaldi and Rutqvist, 2013). Analysis of 3D seismic images also confirmed the presence of such a linear feature at reservoir depth (Gibson-Poole and Raikes, 2010; Wright, 2011). Recent numerical studies by Rinaldi and Rutqvist (2013) showed in more detail that this linear feature (modeled as a fracture zone near KB-502) is confined within the caprock, unlikely to have resulted in CO_2 leakage into the overlying aquifer. Assuming a fracture zone of limited height, previous studies were able to match most available field observations, including the transient evolution of uplift and pressure, as well as the shape of surface deformations. However, such previous studies did not address the error associated with parameter estimation, and no sensitivity analysis was performed to properly assess the relation between these uncertain parameters and predicted state variables.

In the second part of this paper we perform inverse modeling of the injection and related ground surface uplift at injection wells KB-501 and KB-503. The earliest numerical simulations of KB-501 and KB-503 by Rutqvist et al., (2010), showed a good agreement between observations and simulations in terms of maximum surface uplift, without considering the extension of the fracture within the sealing formation. Recently Rucci et al. (2013), using more comprehensive surface deformation data including vertical and horizontal displacement components, showed that an extensional opening might have occurred within the caprock at injection wells KB-501 and KB-503, similarly to KB-502. Here we present inverse modeling results assuming both intact and partially fractured caprocks.

Starting from the results achieved by Rinaldi and Rutqvist (2013) on KB-502, we first improve the forward model with TOUGH-FLAC (Rutqvist, 2011) by accounting for a reactivation criterion for the fracture zone and the injection reservoir. We also account for the changes in permeability associated with the stress evolution. Afterwards, we use our model within an inverse modeling framework of iTOUGH2-PEST (Finsterle and Zhang, 2011), which includes parameter estimation, sensitivity and uncertainty analyses and apply it to all three injection wells

On one hand, the TOUGH-FLAC simulator (Rutqvist, 2011) couples the TOUGH2 simulator for fluid flow in porous media (Pruess et al., 2011) with the FLAC3D simulator for geomechanics and deformation (Itasca, 2009). The applications of TOUGH-FLAC cover geothermal (e.g., Jeanne et al., 2015; Rinaldi et al., 2015a), nuclear waste disposal (e.g., Rutqvist et al., 2014), compressed air storage systems (Rutqvist et al., 2012), shale gas (Rutqvist et al., 2013; 2015), as well as geologic carbon sequestration (Rutqvist et al., 2008; 2010) and related induced seismicity (Cappa and Rutqvist, 2011; Rinaldi et al., 2014a, 2014b, 2015b; Rutqvist et al., 2014, 2016; Urpi et al., 2016). On the other hand, iTOUGH2 (Finsterle, 2004; 2007; Finsterle et al., 2014) has been largely used for sensitivity analysis and parameter estimation for several hydrogeological application (e.g., Doetsch et al., 2013; Finsterle et al., 2013; Poskas et al., 2014; Wainwright et al., 2013; Yuan et al., 2015). Thanks to the PEST protocol (Doherty, 1994), the use of the inverse capabilities of iTOUGH2 can be extended to any numerical forward model; here, we apply for the first time the code iTOUGH2-PEST (Finsterle and Zhang, 2011) to a coupled fluid flow and geomechanics application.

2. FIELD DATA AND MODELING APPROACH

2.1 Data from the In Salah CO_2 storage site

Several data sets were collected at In Salah before and during injection. The principal stress orientation as well as the velocity model was obtained from seismic surveys and well log analyses, while *in-situ* leak-off tests provided the minimum stress magnitude (Gibson-Poole and

Raikes, 2010; Iding and Ringrose, 2010; Wright, 2011; Gemmer et al., 2012; Shi et al., 2012; White et al., 2014).

Although these analyses are extremely useful to set model properties, the transient evolution of uplift as well as injection rates and well pressures play a crucial role in developing a well-constrained coupled fluid flow and geomechanical model. Fig. 1a shows an InSAR image (MDA/Pinnacle Technologies, Wright, 2011) of the rate of satellite-to-ground distance change between November 2003 and March 2010. The CO_2 injection caused a ground surface uplift up to 20 mm after about 6 years of injection activity. The transient evolution of ground-surface displacement along the satellite's Line of Sight (LOS) for the three injection wells is shown in Fig. 1b, for a point located near the maximum uplift. We observe an almost linear increase in uplift for injection wells KB-501 (orange line) and KB-503 (cyan line), reaching about 20 mm and 15 mm in 2010, respectively. The transient evolution at KB-502 (red line) shows that the uplift undergoes a strong increase after the first few months of injection (up to about 15 mm in 1 year), followed by a slower subsidence rate after shut in in mid-2007. Such transient evolution (Fig. 1b) is used as observation for the inverse modeling, accounting for a standard deviation of 2 mm (Donald Vasco, LBNL, personal communication).

A detailed view of the uplift at the three wells after about 2 years of injection (December 23, 2006) is shown in Figs. 1c-e. A bell-shaped, slightly elongated pattern of deformation arises for KB-501 and KB-503 (Fig. 1c and 1e, respectively), and (as mentioned above), some authors suggest that this deformation may result from a fracture zone opening at depth (Rucci et al., 2013). In both cases, LOS displacement reaches about 8 mm of deformation at 500 m SE of the injection well and is about 4 mm and 2 mm along a profile 1700 m SE of the injection well for KB-501 and KB-503, respectively (Fig. 1f and 1h). Fig. 1d shows the above-mentioned double-lobe feature that was observed at KB-502. This pattern of deformation has been interpreted as arising from a vertical feature opening at depth of injection (Vasco et al., 2010; Rutqvist et al., 2011), a feature that was confirmed by 3D seismic images (Gibson-Poole and Raikes, 2010) and corroborated by detailed numerical studies (Rinaldi and Rutqvist, 2013). The double-lobe uplift is also clear in Fig. 1g, which shows the uplift along two profiles. The ground surface reached about 16 mm and 12 mm displacement at 500 m and 1700 m NW of the injection well, respectively. The displacement along these arbitrary profiles (Fig. 1f-h) is used as observational data control for the inverse modeling, and compared to the results of numerical simulations. Also in this case we account for 2 mm standard deviation (Donald Vasco, LBNL, personal communication).

The In Salah storage site was not only characterized by InSAR monitoring. Indeed, wellhead pressure and injection rate were continuously monitored. Fig. 2 shows the injection rate (red line) and the wellhead pressure (black line) monitored at the three wells. The bottomhole pressure (blue line) was calculated from wellhead pressure by using the code T2Well (Pan et al., 2011).

In this study we focus on the injection until August 2008. Fig. 2 shows how CO_2 was continuously injected at KB-501 and KB-503. For KB-502 the injection was suspended in mid-2007 after CO_2 was discovered at the wellhead of a nearby old appraisal well (Mathieson et al., 2011); injection was restarted in mid-2009. The injection was definitively suspended in June 2011 due to concerns about the integrity of the sealing caprock (Ringrose et al., 2013). The injection rates (red line in Fig. 2) are used as input for the model, and the calculated bottomhole pressure (blue line) is used as further observation, to be compared with the numerical results. Regarding the error associated with the bottomhole pressure, we consider a 2 MPa standard deviation, which was calculated using a best fit (cubic relationship) of T2well results accounting for injection rates and wellhead pressure measurements

2.2 Coupled fluid flow and geomechanical forward modeling setup

Forward simulations were carried out with the simulator TOUGH-FLAC (Rutqvist, 2011), which solves hydromechanical problems by sequentially linking the multiphase and multicomponent and heat-transport simulator TOUGH2 (Pruess et al., 2011) with the geomechanical simulator FLAC3D (Itasca, 2009). The sequential approach between the simulators involves data exchange and calculation of parameter variation accounting for THM model. Data from TOUGH2 (namely pressure, temperature, and phase saturation) are passed to FLAC3D for calculation of effective stress and strain variation. Then, data from FLAC3D can be used to compute hydromechanical parameters variation through empirical model (e.g. Rinaldi et al., 2014). Changes in hydromechanical parameters will affect in turn the pressure and stress solution. A detailed formulation can be found elsewhere (Rutqvist, 2011).

The modeling setup presented here closely follows the one proposed by Rinaldi and Rutqvist (2013). Fig. 3 shows the computational domain with *x*-direction corresponding to the NW-SE direction. The hydrogeological model consists of four layers, whose properties are listed in Table 1. The mechanical model is slightly more detailed, accounting for more layers with the hydrogeological caprock section. The mechanical properties, listed in Table 2, closely follow estimates from well log analyses (Gemmer et al., 2012).

Initial temperature and pressure gradients are taken from field investigations. The injection reservoir is at an initial temperature of 90 ˚C with a pore pressure of about 18 MPa. Lateral boundaries are at constant condition, while the bottom boundary is set as a no-flow and no-vertical displacement boundary.

The CO_2 injection takes place in a 20 m thick reservoir at a depth of 1820 m. The injection rates closely following the values shown in Fig. 2, for the corresponding injection well, which was simulated as 1000 m-long.

The medium is poroelastic, with the exception of the storage reservoir and deep fracture zone, both subjected to a failure criterion. The initial stresses also follow field observations, with: σ_{xx}=25.1 MPa/km, σ_{yy}=15.8 MPa/km, and σ_{zz}=22.2 MPa/km.

Following the modeling approach by Rinaldi and Rutqvist (2013), we model, unless otherwise specified, the opening of a deep fracture zone at reservoir depth, extending for 350 m upward into the lower caprock. The length and position of this linear feature closely follow the findings by Rucci et al. (2013). The novelty of the approach presented here consists in the use of a Mohr-Coulomb criterion to determine when such a pre-existing fracture zone reactivates. After reactivation, the tensile opening is simulated by using an orthotropic model.

All the hydraulic and mechanical parameters are constant, with the exception of reservoir permeability and bulk modulus, which change as a function of mean effective stress.

2.2.1 Stress-dependent reservoir permeability and bulk modulus

Compared to the paper by Rinaldi and Rutqvist (2013), the coupled fluid flow and geomechanical formulation is here improved by accounting for the evolution of the reservoir permeability. While the previous work employed a step-wise permeability change, with values in agreement with an analytical solution, here we fully coupled the permeability to the effective stress subjected to a failure condition.

We assume that the injection reservoir is highly fractured and subjected to the Mohr-Coulomb failure criterion for a given friction angle φ_{res}, defined by:

$$f = \sigma_1 - \frac{1+\sin\varphi_{res}}{1-\sin\varphi_{res}}\sigma_3 \qquad (1)$$

When the principal stresses σ_1 and σ_3 within the injection reservoir satisfy the criterion, the permeability and the bulk modulus vary as a function of the mean effective stress.

Several approaches have been proposed to address the relationship between stress and hydromechanical properties, mostly referring to in-situ or laboratory data (Rutqvist, 2015 – and reference therein). Rock permeability is often related to changes in fracture aperture (Whiterspoon et al., 1980), which is generally a function (exponential or inverse relationship) of the normal effective stress (Rutqvist, 2015). Authors have also used such stress-relationships in combination with dilation or slip-tendency approach (e.g. Zhou et al., 2008; Bond et al., 2013).

Here we employed coupling equations based on a relationship between fracture aperture and normal effective stress originally derived by Liu and Rutqvist (2013). Assuming the cubic law (Witherspoon et al., 1980) holds, and referring to the relation between the initial state of stress and the mean effective stress, a stress-dependent permeability can be derived (Rinaldi et al., 2014c):

$$\frac{\kappa}{\kappa_i}=\left(\frac{b}{b_i}\right)^3=\left(\frac{\gamma_e+\gamma_t e^{\frac{\sigma_m^{'}}{K_{t,f}}}}{\gamma_e+\gamma_t e^{\frac{\sigma_{m,i}^{'}}{K_{t,f}}}}\right)^3 \qquad (2)$$

where b and b_i are the current and initial apertures, and κ_{hm} and κ_i are the permeabilities at the current and initial state of stress, respectively. $K_{t,f}$ refers to the bulk modulus of the reservoir fractures, and σ'_m is the effective mean stress. γ_e and γ_t represent the unstressed volume fraction for the hard and soft parts of the rock mass, respectively.

Following Liu and Rutqvist (2013) and assuming a constant bulk modulus for the porous matrix, we have an effective bulk modulus given by:

$$\frac{1}{K_{eff}}=\frac{1}{K_{eff}^{i}}+\Theta_f\frac{\gamma_t}{K_{t,f}}\left(e^{\frac{\sigma_m^{'}}{K_{t,f}}}-e^{\frac{\sigma_{m,i}^{'}}{K_{t,f}}}\right) \qquad (3)$$

where K_{eff} and K^i_{eff} are the current and the initial bulk modulus, respectively, and Θ_f is the volume fraction occupied by fractures, assumed to be 1%.

3.1 Inverse modeling with iTOUGH-PEST and TOUGH-FLAC

The program iTOUGH2 is used as parameter estimation and optimization framework for the TOUGH-FLAC coupled fluid flow and geomechanics simulator. The coupling approach between the two codes is illustrated in Fig. 4. A parameter set estimation is performed in a series of iterations. For a single iteration, parameters to be calibrated (such as permeability, coupling parameters, and/or mechanical parameters) are given by iTOUGH2, which calls a PEST protocol to write input files needed for running TOUGH-FLAC. After completion of the forward run, a PEST protocol follows instructions to extract from the forward model output files. Finally the simulated values are analyzed in iTOUGH, which computes residuals with observation and calculates the parameters set for the next iteration.

In iTOUGH2, residuals are computed as the difference between the measured and simulated observation (here including pressure and uplift in time and space):

$$r_i = z_i^{¿} - z_i \qquad (4)$$

where z_i^* is the *i*-th measured observation and z_i is the *i*-th simulated observation. An overall measure of the misfit between the data and the model is given by a so-called objective function, which here is considered as the least-squares function:

$$S = \sum_{i=1}^{m} \frac{r_i}{\sigma_{zi}^2} \qquad (5)$$

where σ_{zi}^2 is the variance associated with the *i*-th observation, and *m* represents the total number of observations. The best estimated parameter set is the one that minimize such objective function, and the error estimation on the estimated parameters is given by the topology of the objective function around its minimum. In this work we use a Levenberg-Marquardt algorithm to minimize the objective function. Among the iTOUGH2 capabilities, there is also the possibility to evaluate the sensitivity coefficients showing the impact of a small parameter change on the model results.

The main advantage of an inverse modeling approach it is not only limited to the estimation of the unknown parameters, but it can also provide uncertainties on such parameters providing a range of suitable values reproducing the observation. Exploring the uncertainty ranges in estimated parameters constitutes a significant step compared to the previous work (e.g. Rinaldi and Rutqvist, 2013). Moreover the enhanced sensitivity analysis performed during inversion helps choosing the most relevant and critical parameters, giving insights on the processes occurring at depth.

3. INVERSE MODELING FOR KB-502 INJECTION WELL

3.1 Parameter estimation

In this section we focus on the application of the approach for inverse modeling with iTOUGH2-PEST and TOUGH-FLAC to study the injection and deformation at well KB-502. Inverse modeling is conducted to estimate the values for some of the mechanical and hydraulic properties that minimize the misfit between simulated and observed data. For injection well KB-502, Rinaldi and Rutqvist (2013) were able to reproduce the observed uplift and pressure evolution with reasonable detail. However, the unknown parameters were estimated to obtain a reasonable match, and might not have constituted a unique solution. Here we extend the previous finding with a more accurate parameter estimation, error analysis, and sensitivity of the results to parameter variations.

Parameters to be estimated for injection well KB-502 are: (i) friction angle of the injection reservoir, (ii) friction angle of the deep fracture zone, (iii) bulk modulus for stress-dependent permeability (Eq. 2), and (iv-vi) the three Young's moduli in the three directions for the deep fracture zone (E_x, E_y, and E_z), as needed for an orthotropic model. Initial guesses for the parameters can be found in Table 3; they closely follow the values by Rinaldi and Rutqvist

(2013). The initial permeability of the injection reservoir is not considered an adjustable parameter; it was taken from the previous work.

Simulation results are compared with four field observations, as described above: (i) bottom-hole pressure, (ii) transient evolution of the LOS displacement on a single point located above the injection well, and (iii) and (iv) two different profiles located at 500 m and 1700 m, respectively, northwest and parallel to the injection well (Figs. 1 and 2).

We use the Levenberg-Marquardt algorithm to minimize the misfit between model results and field data. A reasonably good match was achieved with six iterations.

The best estimate for the parameters after inversion can be found in Table 3. All the parameters are estimated with a relative error smaller than 1%, with values consistent with previous numerical results. The weighted least-square objective function is reduced from an initial value of 1189.6 to 99.23, and the maximum weighted residual it reduced from about 45 to 15.

Fig. 5 shows the comparison between model results and field observations. We find an excellent match for the bottomhole pressure (Fig. 5a), with the simulated pressure (orange line) consistent with one standard deviation from field observations (2 MPa, gray area). Major differences are found after shut-in, probably related to the fact that the model only accounts for the open section of the well. Fig. 5b and 5c show the comparison between simulated and observed LOS ground surface uplift, along the two profiles. Also in this case we achieve a good match, although we overestimate the uplift in the region far from the double-lobe region. Finally, Fig. 5d shows the resulting transient evolution of the LOS displacement at a single point. The simulated evolution is in excellent agreement with the observed data within one standard deviation (2 mm, gray area. For completeness, we also show the comparison between the simulated and observed pattern of deformation (Fig. 6). Although we do not use the entire map as observation for the inverse analysis, Fig. 6 shows how the simulation is able to reproduce the observed double-lobe uplift.

3.2 Sensitivity analysis

The results of a local sensitivity analysis are summarized in Fig. 7, which shows sensitivity coefficients scaled by the expected parameter variation and the measurement error as a function of time. Further information about the scaling of sensitivity coefficients can be found elsewhere (Finsterle, 2015). Fig. 7a shows that the bottomhole pressure is very sensitive to a change in K_t (parameter largely affecting the permeability). The pressure is also affected by mechanical parameters, such as the bulk modulus of the deep fracture zone in vertical direction (E_z). The friction angle of the fracture zone (ϕ_{res}) has a minor effect, visible only at the time of reactivation (around 2006).

Fig. 7b and 7c show the sensitivities for the LOS displacement along the two profiles. As expected, the surface uplift highly depends on the Young's moduli of the deep fracture zone in the three different directions. The profiles are inversely correlated to E_z and directly correlated to E_y, suggesting more opening compared to the uplift of the fracture zone (an increase in the vertical Young's modulus can be partly compensate by a decrease in the horizontal Young's modulus). It is worth noting that the parameter K_t has also some effect on deformation, suggesting that a coupled fluid and geomechanics model is essential to capture all the features of a complex interacting system. Interestingly, the LOS displacement along the profiles is not sensitive to parameter changes in the far field (i.e., 5 km from the injection region along the profile). Finally, Fig. 7d shows the sensitivity analysis for the transient evolution of the LOS displacement. This observation has a sensitivity similar to the one seen for the profiles. However, the transient evolution of the LOS displacement is only slightly sensitive to the chosen parameters before fracture reactivation.

3.3 Residual analysis

The results of the analysis of the misfit between simulations and field observations are shown in Fig. 8. All the simulated results are in very good agreement with the field observations, with residuals within the assumed errors for each observation.

Fig. 8a shows the misfit for the bottomhole pressure. The misfit between simulation and data is limited to the range -2 to 2 MPa (i.e. one standard deviation), with only few exceptions after shut-in. We accounted for such large errors in pressure because the bottomhole pressure is calculated from wellhead pressures and the injection rate by using the code T2Well. Conceptual and parametric uncertainties in the wellbore simulator increase the expected residual between calculated and measured wellhead pressure. For the LOS displacement along the profiles, the misfit is limited to the range between -2 and 2 mm for most of the observations. Residuals are small in the double-lobe region (less than 2 mm), and increase in the far field, probably due to vertical expansion of the underburden, which has a non-zero permeability (10^{-19} m^2) and it might get pressurized over the 2 years injection (Fig. 8b and 8c). It is also worth noting that our model does not account for possible hydrogeological heterogeneities that may affect the pressure distribution in the injection reservoir. The analysis of the residuals for the temporal evolution of LOS displacement shows that the misfit between simulation and field data is always smaller than the 2 mm error associated with InSAR measurements (Fig. 8d).

4. APPLICATION TO INJECTION WELLS KB-501 AND KB-503

4.1 Inversion cases

Simulations at KB-501 and KB-503 are presented here to understand whether a fracture zone, similar to the one observed at KB-502, might have been reactivated at depth. For both injection wells we performed three inversions. The first inversion does not account for the presence of a fracture zone, and follows a simpler formulation with an intact caprock as used in the first In

Salah modeling by Rutqvist et al. (2010). The parameters estimated in this inversion are: (i) initial permeability, (ii) friction angle of the injection reservoir, (iii) bulk modulus for stress-dependent permeability (Eq. 2), and (iv) permeability of the caprock. The second inversion accounts for a reactivating fracture zone, whose dimensions closely follow the results by Rucci et al. (2013). Such a fracture zone can reactivate subject to a Mohr-Coulomb failure criterion, and once reactivated is modeled as an orthotropic elastic material, similarly to KB-502. For this inversion case, the following parameters are estimated: (i) initial permeability and (ii) friction angle of the injection reservoir, (iii) bulk modulus for stress-dependent permeability (Eq. 2), (iv) friction angle of the fracture zone, and (v-vii) the three Young's moduli in the three directions for the deep fracture zone. Finally, the third inversion case accounts for a deep opening that is pre-active at the start of injection operations; therefore, we do not consider the friction angle of the fracture zone as an adjustable parameter for this inversion case.

4.2 Inverse modeling of KB-501 injection well

The results of the inversion for injection well KB-501 for the three cases are summarized in9. 8, while the estimated parameters are listed in Table 4. The three inversion cases result in equally good matches as measured by the objective function (about 500). The maximum weighted residual has a value of about 35 for the inversion without considering a fracture zone, while it increases up to about 100 for both cases with a fracture zone.

The inversions result in an overall agreement between simulated and calculated bottohole pressure, with residuals within on standard deviation (2 MPa) for all the three cases, and only few minor different among them (Fig. 9a). Although the inversions capture the general trend, the numerical results highly overestimate the pressure at early stage, i.e. before the reservoir permeability starts to change following Eqs. 1 and 2. Afterward the pressure decreases, following the general trend observed in the field, although underestimating the observation in the period between 2007-2008. Figs. 9b and 9c show the resulting LOS displacement along two chosen profiles in comparison with the observed LOS deformation (Fig. 1g). Results suggest that a model without fracture may better reproduce the observations: indeed for the profile at 500 m, only the model with intact caprock is able to simulate the observed trend (Fig. 9b, orange line), while the model with fracture overestimates or underestimates the LOS displacement, for the case of fracturing and pre-fractured caprock, respectively (Fig. 9b purple and green lines). For the profile at 1700 m, the models with pre-fractured and intact caprock are similar (Fig. 9c orange and green lines, respectively), while the case of fracturing caprock results in an overestimated LOS displacement (Fig. 9c purple line). The model with intact caprock also well reproduces the observations throughout the entire simulation (Fig. 9d, orange line), within the associated standard deviation of 2 mm (gray area). The model with a reactivating fracture well represents the first month of injection (Fig. 9d purple line), while the model with pre-active fracture is able to reproduce the observation at late stage (Fig. 9d, green line).

The model with intact caprock seems to better reproduce the observed evolution, according to the results of the numerical inversion. However, the shape of deformation at the surface does not capture the observed pattern of LOS displacement. Indeed, as shown in Fig. 10, only a model with a fracture zone is able to reasonably well represent the observed pattern of deformation (i.e., elongated bell-shaped, Fid. 10c-d). The model with a pre-active fracture zone is also able to reproduce the overall average LOS displacement (i.e., around 9 to 10 mm).

4.2 Inverse modeling of KB-503 injection well

The inversions for KB-503 result in findings similar to what is observed for injection well KB-501. The results for the three cases analyzed are shown in Fig. 11. For this injection well, the pressure is slightly underestimated, especially for the case of the reactivating fracture (Fig. 11a, purple line). The cases of intact caprock and pre-active fracture zone well reproduce the observation within the associated standard deviation of 2 MPa (Fig. 11a, orange and green lines, respectively). In terms of uplift, the case of an intact caprock well reproduces the maximum observed LOS displacement (Fig. 11b and 11c, orange line), while both models with fracture zones largely overestimate the displacement along the profiles (Fig. 11b and 11c, purple and green lines), with a simulated LOS displacement up to 15 mm, compared to the measured value of 9 mm. Finally, all the models fail to properly reproduce the transient evolution of the LOS displacement. In fact, while the observed variation presents a slight subsidence phase during active injection, all models simulate a somewhat linear increase in uplift. Although the observed subsidence can also be interpreted as related to the selected monitoring point, and it could vary quite a lot with the location, the final simulate uplift overestimate between 5 and 10 mm.

Similar to the case of KB-501, the model with intact caprock seems the most appropriate, given the lowest value of the objective function for the analyzed observations. However, also for KB-503, the pattern of deformation simulated for the case of intact caprock does not match the observation (Fig. 12b), while a model with fracture is able to reproduce the elongate bell-shape pattern of deformation (Fig. 12c and 12d).

5. CONCLUSIONS

We conducted joint inversions of coupled fluid flow and geomechanics associated with the CO_2 storage operations, accounting for the large amount of data collected at the In Salah on-shore demonstration site. Starting from numerical simulations performed in the past, we improved the forward model with TOUGH-FLAC. We then performed for the first time an inverse analysis using iTOUGH2-PEST to estimate uncertain parameters of a coupled fluid flow and geomechanics simulation. We also evaluated the error associated with the estimated parameters, and studied the sensitivity of the model output to the parameters of interest. This key step in estimating the uncertainties on critical parameters constitutes the key novelty of the current approach compared to previous models (e.g. Rinaldi and Rutqvist, 2013).

In the first part of this work, we applied the approach to the case of the KB-502 injection well. A model reproducing most of the observed transient data for this injection well was already presented in past works. We used the previous model to test our approach, but accounted for an improved relationship between stress and permeability. Results show that the inverse modeling approach is able to fit the observations after only a few iterations. A sensitivity analysis on the chosen parameters shows that hydraulic parameters (e.g., stress-dependent permeability parameters) may influence geomechanical observations. Results also show that the hydraulic observations (e.g., bottomhole pressure) depend on mechanical parameters, such as the bulk modulus of the fracture zone at depth. Such coupling between variables justifies the use of a coupled fluid flow and geomechanics model to study CO_2 sequestration.

In the second part of this work, we tried to apply the approach to the injection wells KB-501 and KB-503. For these two wells the interpretation of the observed deformation is ambiguous, and some authors have suggested that a fracture zone might have been opened, similarly to KB-502. We investigated three different cases: (i) intact caprock, (ii) reactivating fracture zone, and (iii) pre-active fracture zone. Results for the injection well KB501 and KB-503 suggest that a model with an intact caprock can better reproduce the observations included in the modeling approach: transient evolution of LOS displacement and pressure, as well as the uplift along two arbitrarily chose profile at a specific time (about 2.5 years). However, although not formally accounted for in the inversions, the shape of deformation can only be obtained with a model accounting for a fracture zone, although overestimating (or underestimating) the observed LOS displacement. The reason for overestimating displacements most likely lies in the representation of the fracture zone: the current model simulates the entire fracture zone as reactivating simultaneously, while in the real field a transient process might have occurred. A secondary factor that could affect the uplift is the expansion of the underburden, which might get pressurized over 4 years injection given its permeability (10^{-19} m^2). These effects were probably negligible for KB-502, where the uplift rate was much faster compared to the other wells (Fig. 1b). Furthermore the fracture might have propagated in only one direction, before affecting the entire structure.

Other authors also suggested that an anisotropic permeability field within the reservoir might have played a role in giving a preferential direction for the pressure distribution, which then would have caused the observed elongated shape of deformation that was observed at KB-501 and KB-503 (Shi et al., 2013).

The current inverse modeling approach, coupling iTOUGH2-PEST with TOUGH-FLAC, is a powerful tool to estimate unknown properties for complex coupled fluid flow and geomechanics problems, providing the errors and sensitivities associated with such properties. Future work may include the study and parameterization of the deep fracture zone geometry, as well as the study of the effect of mesh discretization.

ACKNOWLEDGMENTS

This work was supported by the Assistant Secretary for Fossil Energy, Office of Natural Gas and Petroleum Technology, through the National Energy Technology Laboratory, under the U.S. Department of Energy Contract No. DE-AC02-05CH11231. A. P. Rinaldi is currently funded by SNSF Ambizione Energy grant (PZENP2_160555) Technical review comments by Luca Urpi at SED are greatly appreciated. The authors would like to thank the In Salah JIP and their partners BP, Statoil, and Sonatrach for providing field data and technical input over the past 8 years as well as for financial support during LBNL's participation in the In Salah JIP, 2011–2013.

REFERENCES

Bissell, R. C., Vasco, D. W., Atbi, M., Hamdani, M., Okwelegbe, M., Goldwater, M.H., 2011. A full field simulation of the In Salah gas production and CO2 storage project using a coupled geomechanical and thermal fluid flow simulator. *Energy Procedia* 4, 3290–3297.

Bond, C. E., Wightman, R., Ringrose, P.S., 2013. The influence of fracture anisotropy on CO_2 flow, *Geophys. Res. Lett.*, 40, 1284–1289, doi: 10.1002/grl.50313.

Cappa, F., Rutqvist, J., 2011a. Impact of CO_2 geological sequestration on the nucleation of earthquakes. *Geophys. Res. Lett.* 38, L17313. doi:10.1029/2011GL048487.

Doherty, J., 1994. PEST: a unique computer program for model-independent parameter optimisation. In: *Water Down Under 94: Groundwater/Surface Hydrology Common Interest Papers*; Preprints of Papers. Barton, ACT: Institution of Engineers, Australia, 551-554.

Doetsch, J., Kowalsky, M.B., Doughty, C., Finsterle, S., Ajo-Franklin, J.B., Carrigan, C.R., Yang, X., Hovorka, S.D., Daley, T.M., 2013. Constraining CO_2 simulations by coupled modeling and inversion of electrical resistance and gas composition data, *Int. J. Greenh. Gas Contr., 18*, 510-522.

Finsterle, S., 2004. Multiphase inverse modeling: Review and iTOUGH2 applications, *Vadose Zone J.*, 3, 747-762.

Finsterle, S., 2007. *iTOUGH2 User's Guide*, Report LBNL-40040, Lawrence Berkeley Natl. Lab., Berkeley, CA, USA.

Finsterle, S., 2015. Practical notes on local data-worth analysis, *Water Resour. Res.*, *51*(12), 9904–9924, doi: 10.1002/2015WR017445.

Finsterle, S., Zhang, Y., 2011. Solving iTOUGH2 simulation and optimization using PEST protocol, *Environ. Modell. Softw.*, 26(7), 959-968.

Finsterle, S., Zhang, Y., Pan, L., Dobson, P., Oglesby, K., 2013. Microhole arrays for improved heat mining from enhanced geothermal systems, *Geothermics, 47*, 104-114.

Finsterle, S., Sonnenthal, E.L., Spycher, N., 2014. Advances in subsurface modeling: The TOUGH suite of simulators, *Comput. Geosci., 65*, 2-12.

Gemmer, L., Hansen, O., Iding, M., Leary, S., Ringrose, P., 2012. Geomechanical response to CO_2 injection at Krechba, In Salah, Algeria, *First Break*, 30, 79-84.

Gibson-Poole, C.M., Raikes, S., 2010. Enhanced understanding of CO_2 storage at Krechba from 3D seismic, *9^{th} Annual Conference on Carbon Capture and Sequestration*, Pittsburgh, PA, USA, Ma 10-13, 2010.

Iding, M., Ringrose, P., 2010. Evaluating the impact of fractures on the performance of the In Salah, CO_2 storage site, *Int. J. Greenh. Gas Contr.*, 4, 242-248.

ITASCA, 2009. *FLAC3d v5.0, Fast Lagrangian Analysis of Continua in 3 Dimensions, User's Guide*, Itasca Consulting Group, Minneapolis, MN, USA.

Jeanne, P., Rutqvist, J., Rinaldi, A.P., Dobson, P.F., Walters, M., Hartline, C., Garcia, J., 2015. Seismic and aseismic deformations and impact on reservoir permeability: The case of EGS stimulation at The Geysers, California, USA, *J. Geophys. Res. – Solid Earth*, 120, 7863–7882, doi:10.1002/2015JB012142.

Jha, B., Juanes, R., 2014. Coupled multiphase flow and poromechanics: A computational model of pore pressure effects on fault slip and earthquake triggering. *Water Res. Res.* 50(5), 3776-

3808.

Kolditz, O., Bauer, S., Bilke, L., Böttcher, N., Delfs, J.O., Fischer, T., Görke, U.J.,Kalbacher, T., Kosakowski, G., McDermott, C.I., Park, C.H., Radu, F., Rink, K., Shao, H., Shao, H.B., Sun, F., Sun, Y.Y., Singh, A.K., Taron, J., Walther, M., Wang, W.,Watanabe, N., Wu, Y., Xie, M., Xu, W., Zehner, B., 2012. OpenGeoSys: an open-source initiative for numerical simulation of thermo-hydro-mechanical/chemical (THM/C) processes in porous media, *Environ. Earth Sci.* 67(2), 589-599.

Liu, H.H., Rutqvist, J., 2013. Coupled hydromechanical processes associated with multiphase flow in a dual-continuum system: formulations and an application, *Rock Mech. Rock Eng.*, 46(5), 1103-1112.

Mathieson, A., Midgley, J., Wright, I., Saoula, N., Ringrose, P., 2011. In Salah CO_2 storage JIP: CO_2 sequestration monitoring and verification technologies applied at Krechba, Algeria, *Energy Procedia*, 4, 3596-3603.

Pacala, S., Socolow, R., 2004. Stabilization wedges: solving the climate problem for the next 50 years with current technologies. *Science* 13305(5686), 968–972.

Pan, L., Oldenburg, C. M., Pruess, K., Wu, Y.-S., 2011. Transient CO_2 leakage and injection in wellbore-reservoir system for geological carbon sequestration, *Greenh. Gas. Sci. Tech.*, 1(4), 335-350.

Poskas, P., Narkuniene, A., Grigaliuniene, D., Finsterle, S., 2014. Comparison of radionuclide releases from a conceptual geological repository for RBMK-1500 and BWR spent nuclear fuel, *Nuclear Techn.*, *185*(3), 32-335.

Pruess, K., Oldenburg, C.M., Moridis, G., 2011. *TOUGH2 User's Guide, Version 2.*1, Paper LBNL-43134 (revised). Lawrence Berkeley Natl. Lab., Berkeley, CA, USA.

Rinaldi, A.P., Rutqvist, J., 2013. Modeling of deep fracture zone opening and transient ground surface uplift at KB-502 CO_2 injection well, In Salah, Algeria, *Int. J. Greenh. Gas Contr.*, 12, 155-167. doi:10.1016/j.ijggc.2012.10.017

Rinaldi, A.P., Rutqvist, J., Cappa, F., 2014a. Geomechanical effects on CO_2 leakage through fault zones during large-scale underground injection. *Int. J. Greenh. Gas Contr.* 20, 171-131. doi:10.1016/j.ijggc.2013.11.001

Rinaldi, A.P., Jeanne, P., Rutqvist, J., Cappa, F., Guglielmi, Y., 2014b. Effects of fault-zone architecture on earthquake magnitude and gas leakage related to CO_2 injection in a multi-layered sedimentary system. *Greenh. Gas Sci. Techn.* 4, 99-120. doi: 10.1002/ghg.1403

Rinaldi, A.P., Rutqvist, J., Finsterle, S., Liu, H.H., 2014c. Forward and inverse modeling of ground surface uplift at In Salah, Algeria, *48th US Rock Mechanics/Geomechanics Symposium*, Minneapolis, MN, USA, 1-4 June.

Rinaldi, A.P., Rutqvist, J., Sonnenthal, E., Cladouhos, T.T., 2015a. Coupled THM Modeling of

Hydroshearing Stimulation in Tight Fractured Volcanic Rock, *Tranp. Por. Med.* 108(1), 131-150. 10.1007/s11242-014-0296-5

Rinaldi, A. P., Vilarrasa, V., Rutqvist, J., Cappa, F., 2015b. Fault reactivation during CO_2 sequestration: effects of well orientation on seismicity and leakage, *Greenh. Gas. Sci. Tech.*, 5, 645-656, doi: 10.1002/ghg.1511.

Rucci, A., Vasco, D.W., Novali, F., 2013. Monitoring the geological storage of carbon dioxide using multicomponent SAR interferometry. *Geophys. J. Int.* 193(1), 197-208.

Ringrose, P.S., Mathieson, A.S., Wright, I.W., Selama, F., Hansen, O., Bissell, R., Saoula, N., Midgley, J., 2013. The In Salah CO_2 storage project: lessons learned and knowledge transfer, *Energy Procedia*, 37, 6226-6236.

Rutqvist, J., 2011. Status of TOUGH-FLAC simulator and recent applications related to coupled fluid flow and crustal deformations. *Comput. Geosci.* 37, 739-750.

Rutqvist, J., 2012. The Geomechanics of CO_2 Storage in Deep Sedimentary Formation. *Geotech. Geol. Eng.* 30(3), 525-551. doi:10.1007/s10706-011-9491-0.

Rutqvist, J., 2015. Fractured rock stress-permeability relationships from in-situ data and effects of temperature and chemical-mechanical couplings. *Geofluids* 12(1-2), 48-66. doi:10.1111/gfl.12089.

Rutqvist, J., Birkholzer, J. T., Tsang, C.-F., 2008. Coupled reservoir-geomechanical analysis of the potential for tensile and shear failure associated with CO_2 injection in multilayered reservoir-caprock systems. *Int. J. Rock Mech. Min. Sci.*, 45(2), 132-143. doi:10.1016/j/ijrmms.2007.04.006.

Rutqvist, J., Vasco, D.W., Myer, L., 2010. Coupled reservoir-geomechanical analysis of CO_2 injection and ground deformations at In Salah, *Int. J. Greenh. Gas Contr.*, 4, 225-230.

Rutqvist, J., Liu, H.H., Vasco, D.W., Pan, L., Kappler, K., Majer, E., 2011. Coupled non-isothermal, multiphase fluid flow, and geomechanical modeling of ground surface deformations and potential for induced micro-seismicity at the In Salah CO_2 storage operation. *Energy Procedia* 4, 3542–3549.

Rutqvist, J., Kim, H. M., Ryu, D. W., Synn, J. H., Song, W. K., 2012. Modeling of coupled thermodynamic and geomechanical performance of underground compressed air energy storage in lined rock caverns. *Int. J. Rock Mech. & Min. Sci.* 52, 71-81. doi:10.1016/j.ijrmms.2012.02.010.

Rutqvist, J., Rinaldi, A. P., Cappa, F., Moridis, G. J., 2013. Modeling of fault reactivation and induced seismicity during hydraulic fracturing of Shale-Gas reservoir. *J. Petrol. Sci. Eng.* 107, 31-44. doi:10.1016/j.petrol.2013.04.023

Rutqvist, J., Zheng, L., Chen, F., Liu, H.H., Birkholzer, J., 2014. Modeling of coupled thermo-hydro-mechanical processes with links to geochemistry associated with bentonite-backfilled repository tunnels in clay formations, *Rock Mech. Rock Eng.*, 47, 167-186. doi: 10.1007/s00603-013-0375-x

Rutqvist, J., Cappa, F., Rinaldi, A.P., Godano, M., 2014. Modeling of induced seismicity and ground vibrations associated with geologic CO2 storage, and assessing their effects on surface structures and human perception. *Int. J. Greenh. Gas Contr.*, 24, 64–77.

Rutqvist, J., Rinaldi, A.P., Cappa, F., Moridis, G.J., 2015. Modeling of Fault Activation and Seismicity by Injection Directly into a Fault Zone associated with Hydraulic Fracturing of Shale-gas Reservoirs, *J. Petrol. Sci. Eng.*, 127, 377-386. doi:10.1016/j.petrol.2015.01.019

Rutqvist, J., Rinaldi, A.P., Cappa, F., Jeanne, P., Mazzoldi, A., Urpi, L., Guglielmi,Y., Vilarrasa, V., 2016. Fault activation and induced seismicity in geologic carbon storage - Lessons learned from recent modeling studies, *J. Rock Mech. Geotech. Eng.*, in press, doi: 10.1016/j.jrmge.2016.09.001.

Shi, J. Q., Sinayuc, C., Durucan, S, Korre, A., 2012. Assessment of carbon dioxide plume behaviour within the storage reservoir and the lower caprock around the KB-502 injection well at In Salah, *Int J. Greenh. Gas Contr.*, 7, 115-126.

Shi, J. Q., Smith, J., Durucan, S., Korre, A., 2013. A coupled reservoir simulation-geomechanical modeling study of the CO2 injection-induced ground surface uplift observed at Krechba, In Salah. *Energy Procedia*, 37, 3719 – 3726.

Urpi, L., Rinaldi, A.P., Rutqvist, J., Cappa, F., Spiers, C.J., 2016. Dynamic simulation of CO_2-injeciton-induced fault rupture with slip-rate dependent friction coefficient, *Geomech. Energy Environ.*, in press. doi: 10.1016/j.gete.2016.04.003

Vasco, D.W., Rucci, A., Ferretti, A., Novali, F., Bissell, R.C., Ringrose, P.S., Mathieson, A.S., Wright, I.W., 2010. Satellite-based measurements of surface deformation reveal fluid flow associated with the geological storage of carbon dioxide, *Geophys. Res. Lett.*, 37, L03303.

Verdon, J.P., Stork, A.L., 2016. Carbon capture and storage, geomechanics, and induced seismic activity. *J. Rock Mech. Geotech. Eng.*, in press. Doi: 10.1016/j/jrmge.2016.06.004

Vilarrasa, V., Bolster, D., Olivella, S., Carrera, J., 2010. Coupled hydromechanical modeling of CO_2 sequestration in deep saline aquifers. *Int. J. Greenh. Gas Control* 4(6), 910-919.

Vilarrasa, V., Carrera, J., 2015. Geologic Carbon Storage Is Unlikely to Trigger Large Earthquakes and Reactivate Faults through Which CO_2 Could Leak. *P. Natl. Acad. Sci. USA* 112(19), 5938–5943.

Wainwright, H.M., Finsterle, S., Zhou, Q., Birkholzer, J.T., 2013. Modeling the performance of large-scale CO2 storage systems: A comparison of different sensitivity analysis methods, *Int. J. Greenh. Gas Contr.*, *17*, 189-205.

Yuan, Y., Khare, Y., Wang, X., Parajuli, P.B., Kisekka, I., Finsterle, S., 2015. Hydrologic and water quality models: Sensitivity, *Trans. ASABE*, 58(6), 1721-1744.

White, J.A., Chiaramonte, L., Ezzedine, S., Foxall, W., Hao, Y., Ramirez, A., McNab, W., 2014. Geomechanical behavior of the reservoir and caprock system at the In Salah CO_2 storage project. *P. Natl. Acad. Sci. USA*, 111(24), 8747-8752.

Witherspoon, P.A., Wang, J.S.W., Iwai, K., Gale, J.E., 1980. Validity of cubic law for fluid flow in deformable rock fracture, *Water Res. Res.*, 16(6), 1016-1024, 1980.

Wright, I., 2011. In Salah CO_2 storage JIP lessons learned, *10th Annual Conference on Carbon Capture and Sequestration*, Pittsburgh, PA, USA.

Zhou, J., Chen, M., Jin, Y., Zhang, G., 2008. Analysis of fracture propagation behavior and fracture geometry using a tri-axial fracturing system in naturally fractured reservoirs, *Int. J. Rock. Mech. Min. Sci.*, 45, 1143-1152, doi: 10.1016/j.ijrmms.2008.01.001

Zoback, M. D., Gorelick, S. M., 2012. Earthquake triggering and large-scale geologic storage of carbon dioxide. *P. Natl. Acad. Sci. USA*, 109(26), 10164-10168.

Tables

Table 1. Hydrogeological properties used in the forward model (Rinaldi and Ruqtvist, 2013). Stress-dependent parameters in bold.

	Depth (m)	Φ_0 (-)	κ_0 (m^2)
Shallow	0-900	0.1	10^{-12}
Caprock	900-1800	0.01	10^{-21}
Reservoir	1800-1820	0.17	**0.8×10^{-14}**
Basement	>1820	0.01	10^{-19}

Table 2. Geomechanical properties based on well log analysis (Gemmer et al., 2012). Depths were slightly modified to fit our geological model (Table 1). Stress-dependent parameters in bold.

Depth (m)	Young's modulus *E* (GPa)	Poisson's ratio □(-)
0-900	3	0.25
900-1650	5	0.3
1650-1780	2	0.3
1780-1800	20	0.25
1800-1820	**10**	0.2
1820-4000	15	0.3

Table 3. Estimated parameters for KB-502 injection well (initial guess E_x, E_y, and E_z from Rinaldi and Rutqvist, 2013).

	Initial Guess	Best estimate
K_t (Pa)	$10^{7.0253}$	$10^{6.90\pm0.01}$ (7.94 MPa)
ϕ_{res} (˚)	31	27.9±0.3
ϕ_{frac} (˚)	31	30.6±0.2
E_x (Pa)	0.17×10^9	$10^{8.71\pm0.05}$ (0.51 GPa)
E_y (Pa)	0.14×10^9	$10^{8.13\pm0.03}$ (0.13 GPa)
E_z (Pa)	10^9	$10^{9.06\pm0.02}$ (1.15 GPa)
Objective func.	1189.6	99.23
Max. Residual	44.89	14.52

Table 4. Estimated parameters for KB-501 injection well. For each inversion the objective function and maximum residual of the initial guess is shown in parenthesis.

	Intact caprock	Fracture zone	Pre-active fracture
κ_{res} (m^2)	$10^{-14.16\pm0.03}$	$10^{-14.41\pm0.02}$	$10^{-14.43\pm0.01}$
κ_{cap} (m^2)	$10^{-23\pm5}$	-	-
ϕ_{res} (˚)	31±0.6	31±1	31±1
K_t (Pa)	$10^{7.3\pm0.1}$ (20.8 MPa)	$10^{7.40\pm0.02}$ (25.1 MPa)	$10^{7.38\pm0.02}$ (23.9 MPa)
ϕ_{frac} (˚)	-	26±1	-
E_x (Pa)	-	$10^{9.68\pm0.03}$ (4.7 GPa)	$10^{9.65\pm0.04}$ (4.5 GPa)

E_y (Pa)	-	$10^{8.76\pm0.01}$ (0.57 GPa)	$10^{8.75\pm0.03}$ (0.56 GPa)
E_z (Pa)	-	$10^{9.70\pm0.01}$ (5.01 GPa)	$10^{9.70\pm0.03}$ (5.01 GPa)
Objective func.	508.35	575.26	544.28
Max. Residual	35.77	106.85	99.19

Table 5. Estimated parameters for KB-503 injection well. For each inversion the objective function and maximum residual of the initial guess is shown in parenthesis.

	Intact caprock	Fracture zone	Pre-active fracture
κ_{res} (m^2)	$10^{-13.77\pm0.05}$	$10^{-14.05\pm0.02}$	$10^{-13.98\pm0.01}$
κ_{cap} (m^2)	$10^{-22\pm1}$	-	-
ϕ_{res} (˚)	29±1	27±2	28.0±0.5
K_t (Pa)	$10^{7.3\pm0.1}$ (20 MPa)	$10^{7.17\pm0.02}$ (25.1 MPa)	$10^{7.39\pm0.03}$ (24.5 MPa)
ϕ_{frac} (˚)	-	30±10	-
E_x (Pa)	-	$10^{9.66\pm0.02}$ (4.6 GPa)	$10^{9.65\pm0.01}$ (4.5 GPa)
E_y (Pa)	-	$10^{9\pm1}$ (1 GPa)	$10^{8.68\pm0.01}$ (0.48 GPa)
E_z (Pa)	-	$10^{10\pm1}$ (10 GPa)	$10^{9.70\pm0.02}$ (5.01 GPa)
Objective func.	554.36	1438.6	1129.4
Max. Residual	47.93	67.23	62.18

Figures

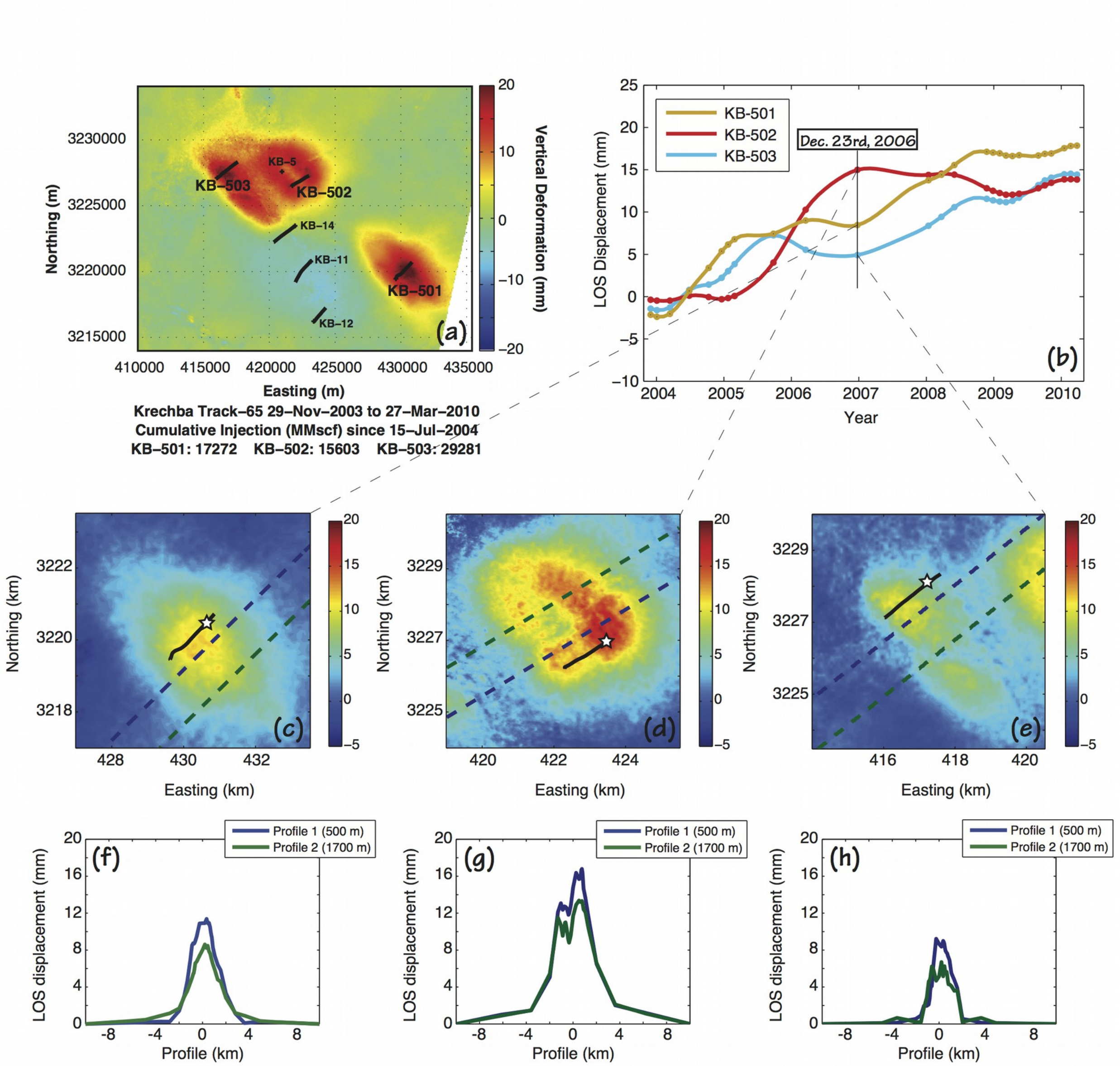

Figure 1. (a) Ground surface uplift at In Salah (image by MDA/Pinnacle Technologies, Wright, 2011). (b) Transient evolution of uplift at the three injection well, used as observations for inverse modeling. The monitoring point is placed at the ground surface at the end of the injection well (c-e) Close view of ground uplift in December 2006 after about 2.5, 1.5, and 2.5 years from starting of injection for wells KB-501, KB-502, and KB503, respectively. The star indicates the monitoring point for the transient evolution used as observation (d-f) Uplift along two profiles at 500 and 1700 m from injection well, respectively, for the three injection wells. Displacement along profiles used as observation for inverse modeling. Figure modified after Rinaldi et al. (2014c).

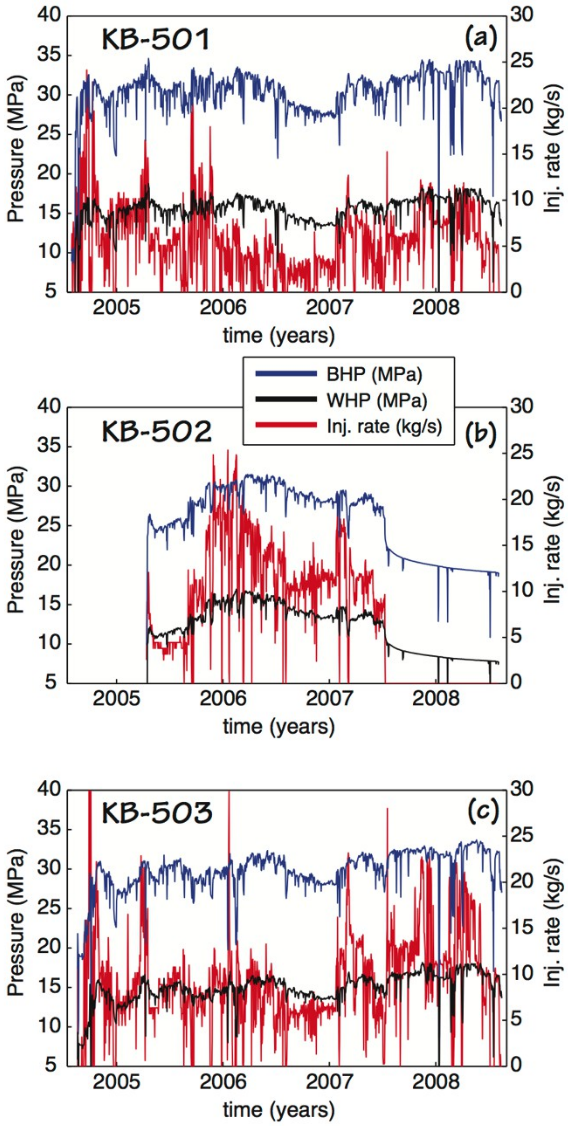

Figure 2. (a-c) Injection rate (red line), measured wellhead pressure (black line), and bottomhole pressure (blue line) for the three injection wells. The bottomhole pressure was calculated with T2Well (Pan et al., 2011). Figure modified after Rinaldi et al. (2014c).

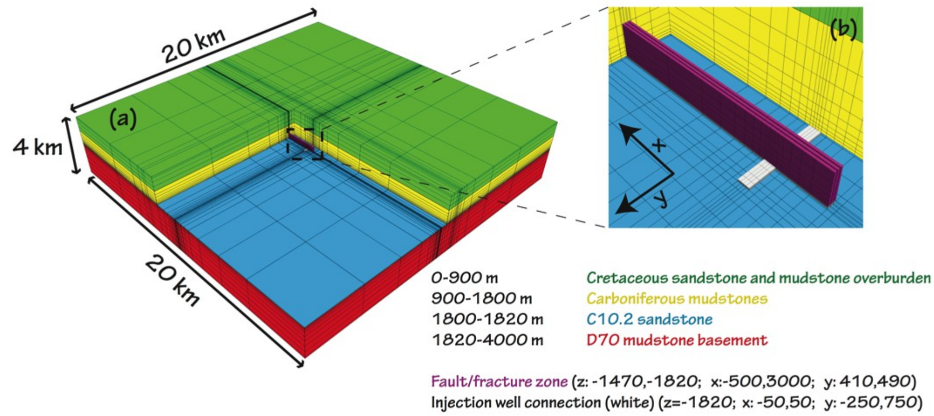

Figure 3. Computational domain. (a) 3D model with four hydrogeological formations. (b) Enlargement of the fracture zone, whose length along the *x*-direction depends on the simulation (modified after Rinaldi and Rutqvist, 2013).

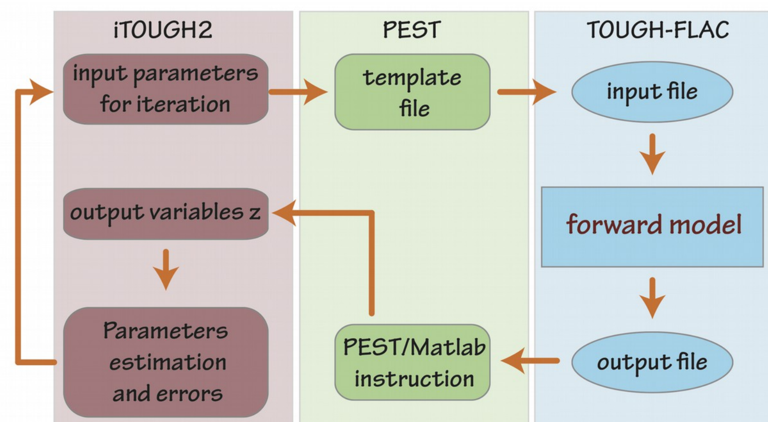

Figure 4. Scheme for inverse modeling iterations in iTOUGH2-PEST with TOUGH-FLAC.

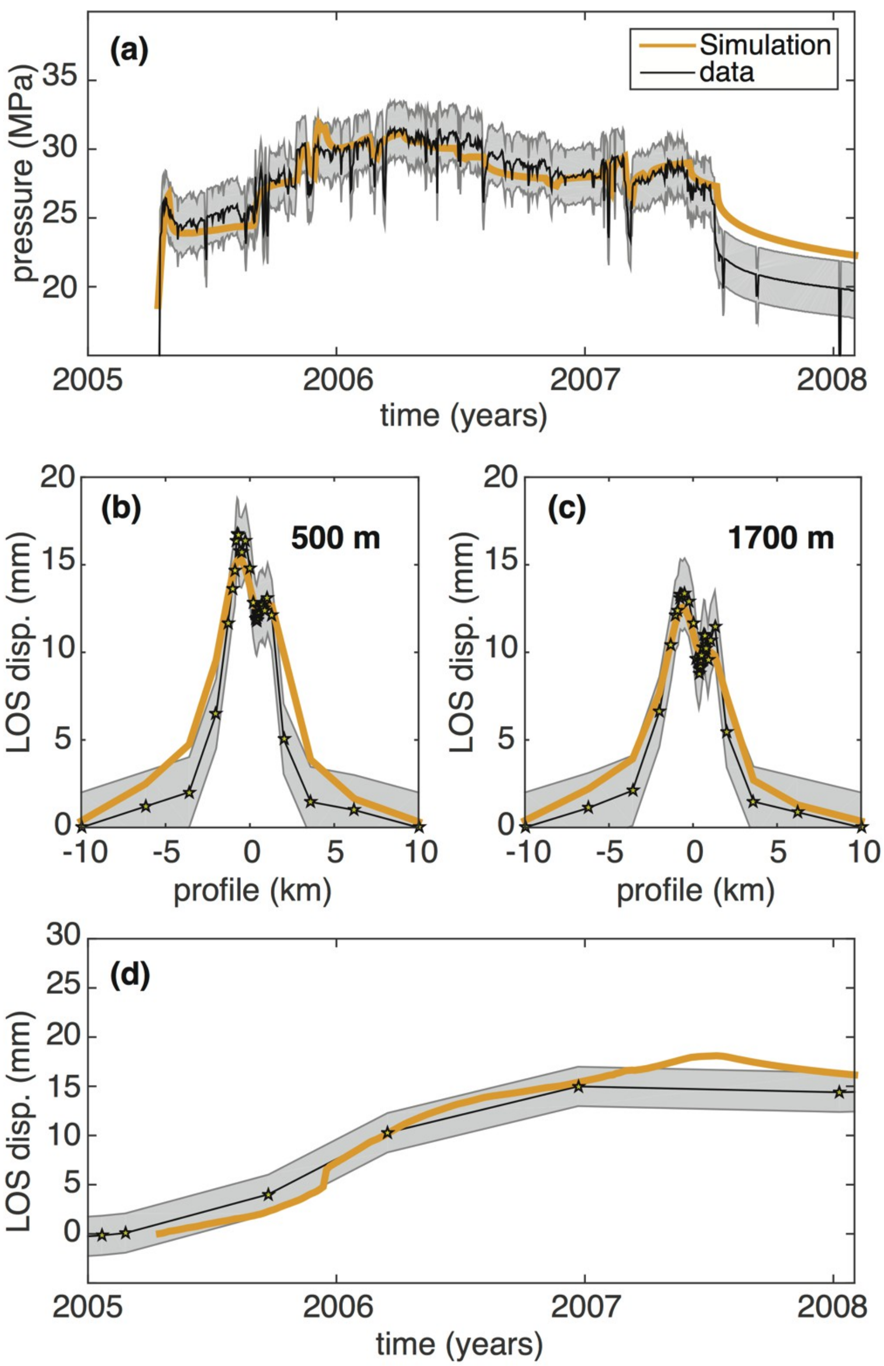

Figure 5. Comparison between simulated and observed data at KB-502: (a) temporal evolution of bottomhole pressure, (b) profile of ground uplift at 500 m after 618 days, (c) profile of ground uplift at 1700 m after 618 days, (d) temporal evolution of ground uplift at a point placed at ground surface at the end of the injection well (Fig. 1d and Fig. 5). The gray area represents the 1 standard deviation (2 MPa and 2 mm for pressure and LOS displacement, respectively).

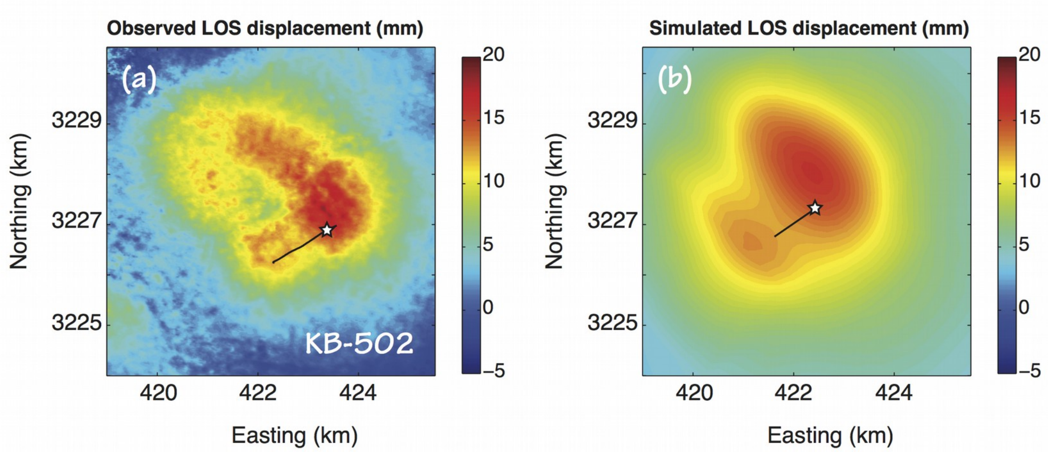

Figure 6. Resulting deformation after inversion for KB-502 injection well. (a) Observed LOS displacement, (b) simulated LOS displacement. The star indicates the monitoring point for the temporal evolution.

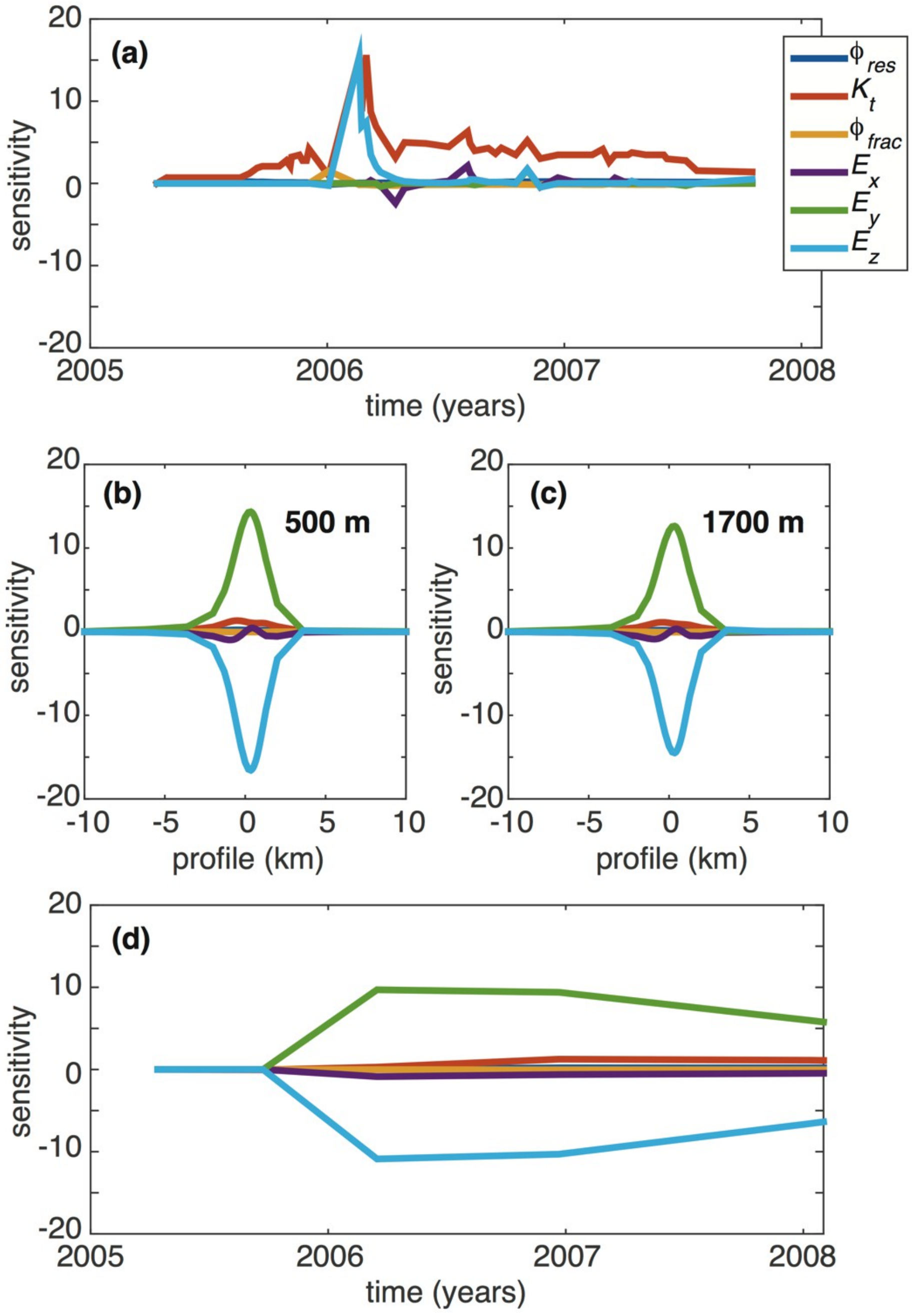

Figure 7. Sensitivity analysis: (a) temporal evolution of bottomhole pressure, (b) profile of ground uplift at 500 m after 618 days, (c) profile of ground uplift at 1700 m after 618 days, (d) temporal evolution of ground uplift.

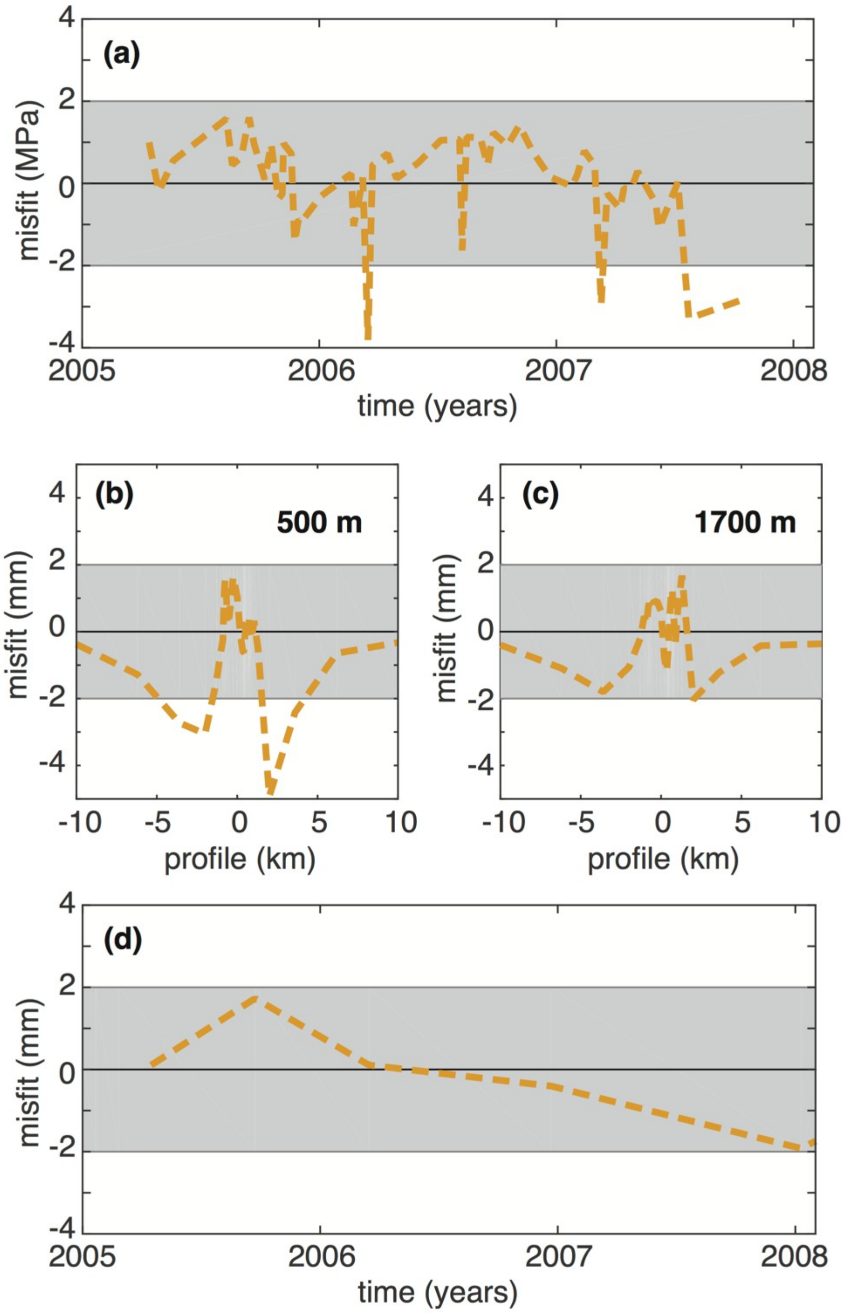

Figure 8. Residual analysis: (a) temporal evolution of bottomhole pressure, (b) profile of ground uplift at 500 m after 618 days, (c) profile of ground uplift at 1700 m after 618 days, (d) temporal evolution of ground uplift.

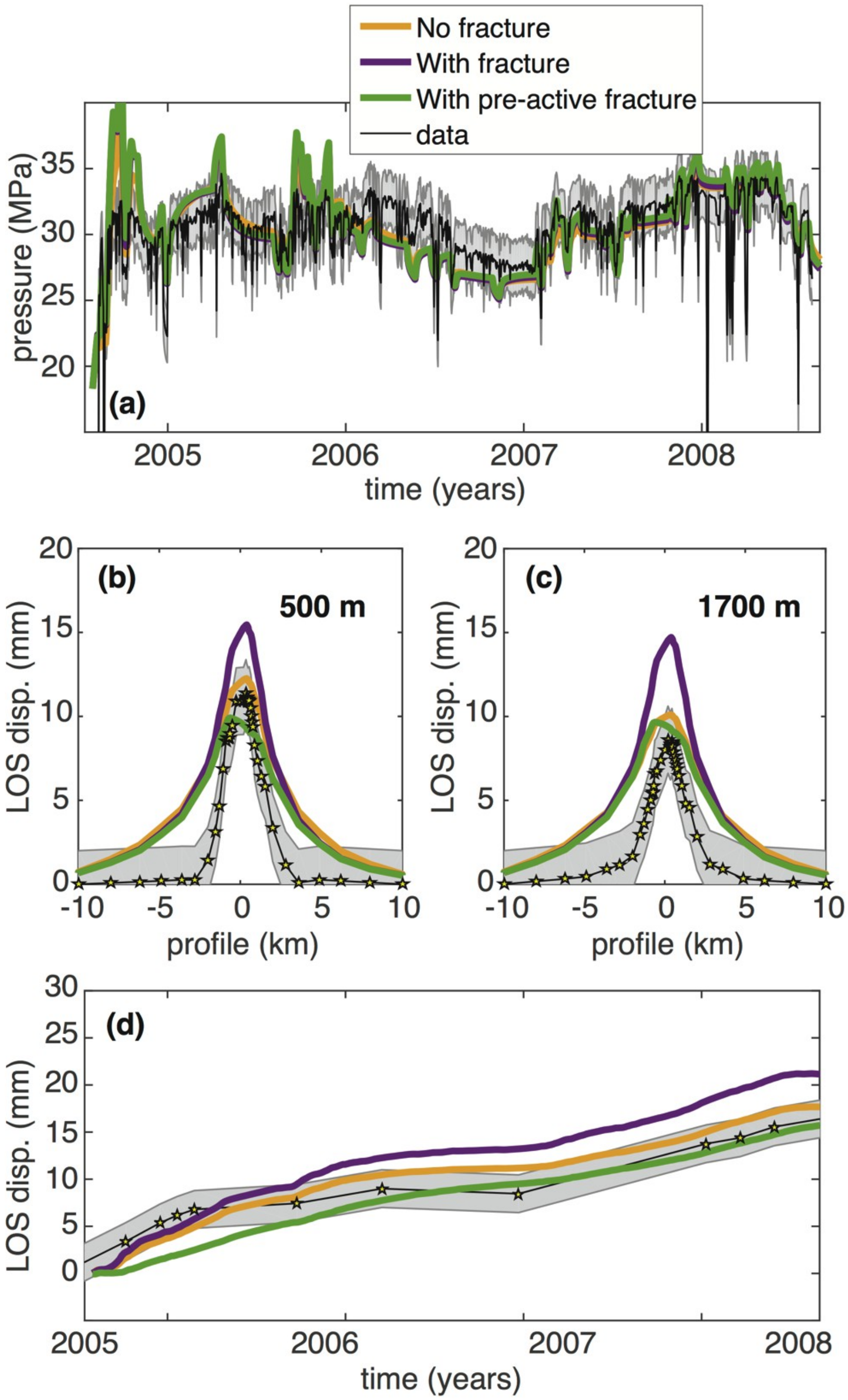

Figure 9. Comparison between simulated and observed data at KB-501: (a) temporal evolution of bottomhole pressure, (b) profile of ground uplift at 500 m after 877 days, (c) profile of ground uplift at 1700 m after 877 days, (d) temporal evolution of ground uplift at a point placed at the end of the injection well (Fig. 1c and Fig. 9). The gray area represents the 1 standard deviation (2 MPa and 2 mm for pressure and LOS displacement, respectively).

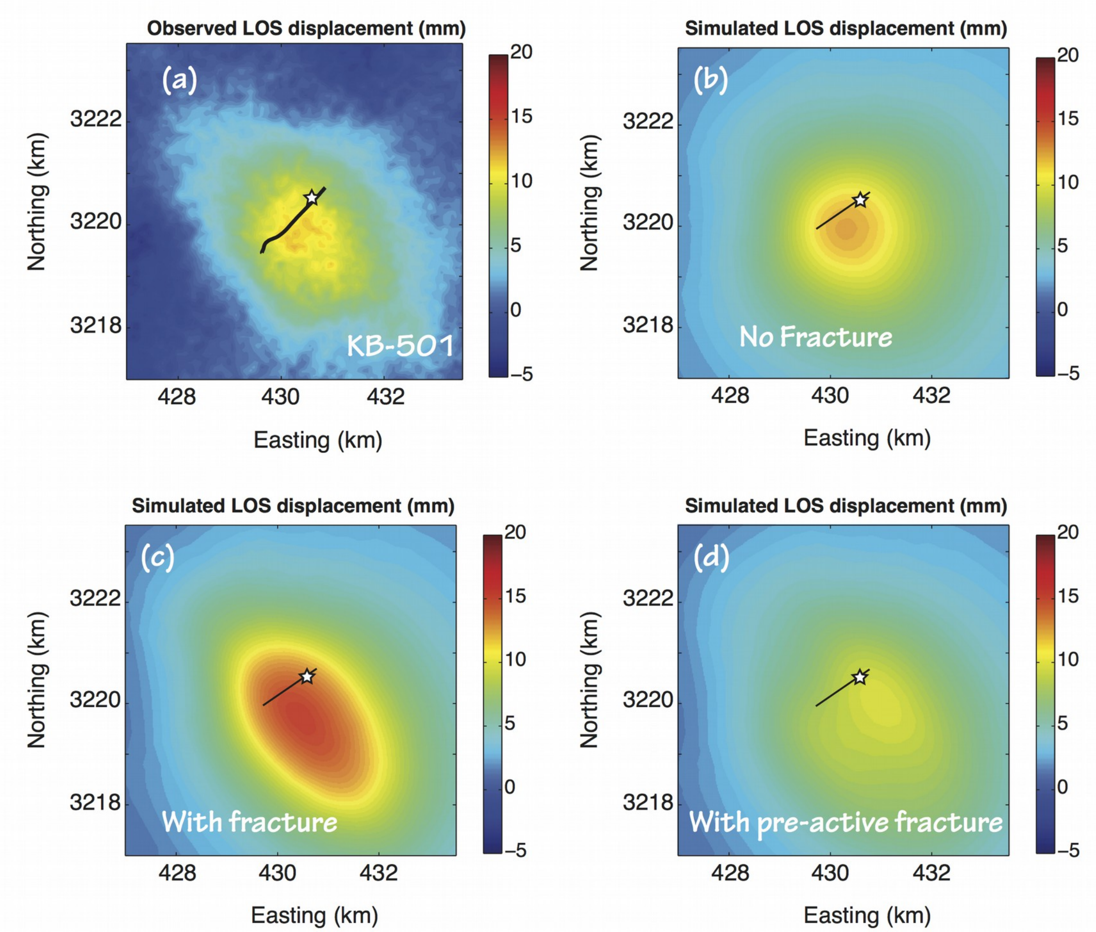

Figure 10. Resulting deformation after inversion for KB-501. Observed and simulated LOS displacement for (b) intact caprock, (c) reactivating, and (d) pre-active fracture zone. The star indicates the monitoring point for the temporal evolution.

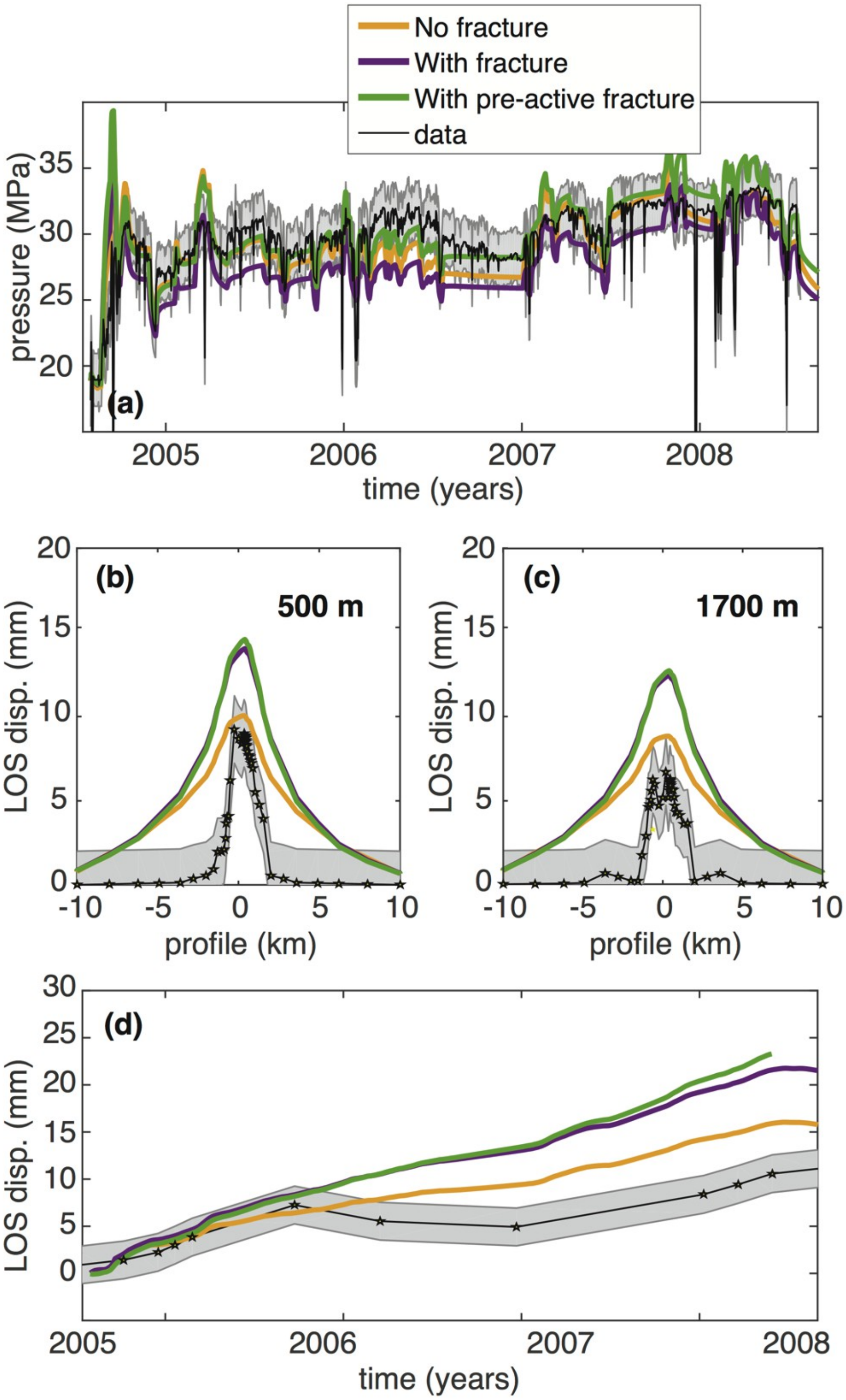

Figure 11. Comparison between simulated and observed data at KB-503: (a) temporal evolution of bottomhole pressure, (b) profile of ground uplift at 500 m after 857 days, (c) profile of ground uplift at 1700 m after 857 days, (d) temporal evolution of ground uplift at a point placed at the end of the injection well (Fig. 1e and Fig. 11). The gray area represents the 1 standard deviation (2 MPa and 2 mm for pressure and LOS displacement, respectively).

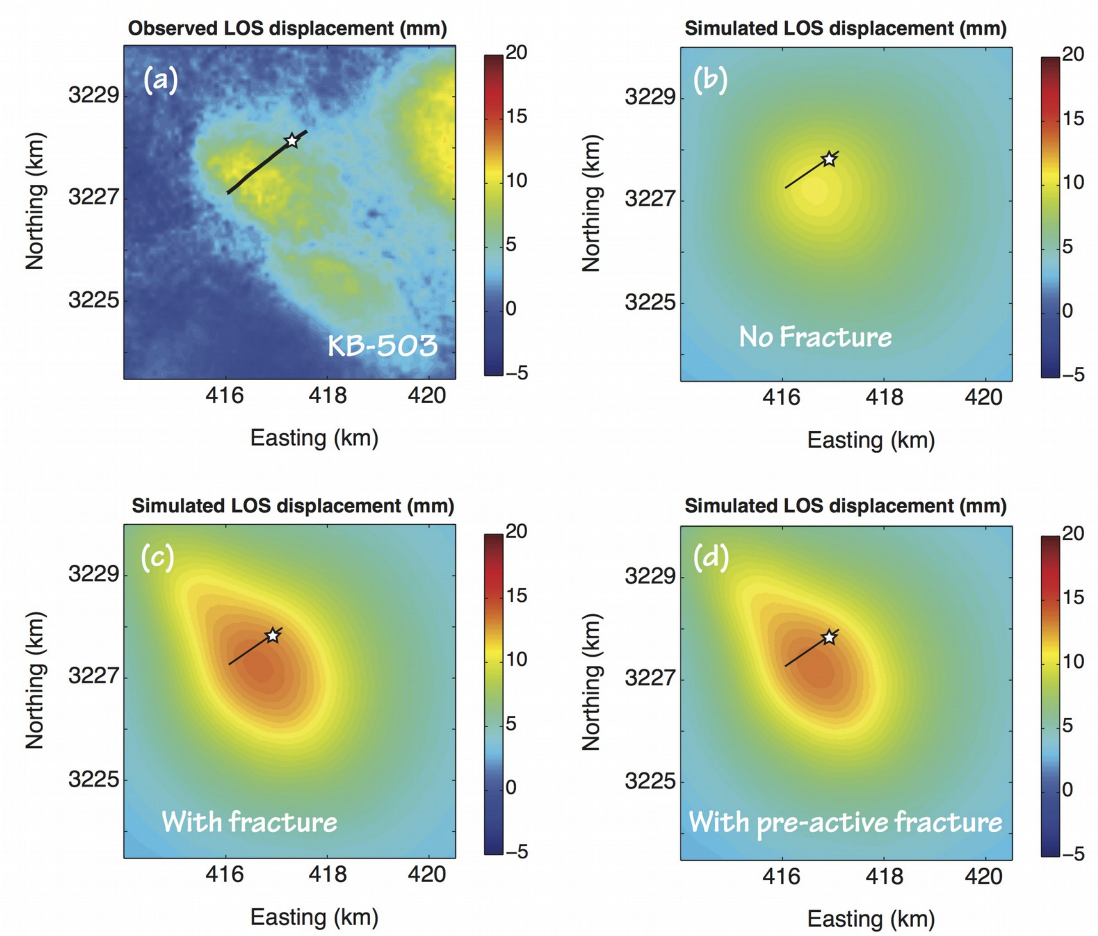

Figure 12. Resulting deformation after inversion for KB-503. Observed and simulated LOS displacement for (b) intact caprock, (c) reactivating, and (d) pre-active fracture zone. The star indicates the monitoring point for the temporal evolution.